Development of the LIPAc ionization profile monitor

J. Egberts, Ph. Abbon, H. Deschamps, F. Jeanneau,
J. Marroncle, J-Ph. Mols, and Th. Papaevangelou
CEA Saclay, Gif sur Yvette, France

(Dated: December 15, 2011)

Abstract

In the frame of the International Fusion Material Irradiation Facility (IFMIF), a prototype for a non-interceptive transverse beam Profile Monitor based on residual gas Ionization (IPM) has been built and characterized in detail. Based on these tests, the final IPM has been designed, built, and tested.

We present the design of the IPM based on FEM (Finite Element Method) field simulations and the results of test measurements performed at GSI Darmstadt with heavy ion beams of up to 1.6 mA at 5 MeV/u and at CEA Saclay with 80 keV protons in a cw high current beam. During the tests, parameters like extraction field strength, residual gas type and pressure, and beam position with respect to the IPM have been varied and the effects on the profile have been evaluated. Beam profiles were investigated with respect to signal intensity and profile shape. A profile comparison with a Beam Induced Fluorescence (BIF) monitor indicates a good agreement of profiles acquired by the two profilers. Finally, the development of a software algorithm is presented that aims to recover profile shapes that are distorted due to the space charge of the beam.

INTRODUCTION

Modern high-power and high-current accelerators often render conventional interceptive diagnostic devices useless as the increased power deposition in the material could destroy the device. This raises increased demands for non-interceptive diagnostic devices like residual gas profilers. Residual gas beam profile monitors take advantage of interactions of the beam with the residual gas inside the vacuum pipe. Interaction processes commonly exploited for profile measurements are ionization and excitation of the residual gas atoms [1]. We report the development of a non-interceptive *Ionization Beam profile Monitor (IPM)* for the LIPAc accelerator.

The *LIPAc (Linear IFMIF prototype Accelerator)* will be a prototype of the *IFMIF (International Fusion Material Irradiation Facility)* accelerator. The IFMIF accelerator will consist of two drivers that each accelerates a 125 mA *continuous wave (cw)* deuteron beam up to 40 MeV and then collide it on a liquid lithium target. This corresponds to a beam power of 10 MW in total. The beam impinging on the lithium target will trigger nuclear reactions in which neutrons are released that can be used to irradiate material samples to test them on their radiation hardness. The LIPAc accelerator will consist of the first part of a single IFMIF driver, i.e. the source, the RFQ and the first cryostat of the superconducting linac. It will have the very same beam characteristics, but the final energy will be limited to 9 MeV only [2].

IONIZATION PROFILE MONITORS

Ionization profile monitors (IPM) measure the ionization of the residual gas by the particle beam. The ionization current can be calculated by

$$I_{Ioniz} = n \cdot d \cdot \sigma_{Ioniz} \cdot I_{Beam} \tag{1}$$

with n being the residual gas particle density, d the interaction length, σ_{Ioniz} being the ionization cross section, and I_{Beam} the beam current. Ionization cross sections still depend on various parameters like projectile velocity, charge state, and residual gas atom type [3], but for most accelerator beams, such parameters can be considered as constant. For such beams, the ionization particle density is directly proportional to the beam current density

which allows for a determination of the accelerator beam profile by measuring the ionization current.

The ionization products, ions or electrons, are extracted from the beam by an electric field. This field is commonly applied by a field box. The ionization products are accelerated by the electric field towards a read-out plate where the profile of the ionization current is measured [4]. For the read-out plate, phosphor screens are frequently chosen, for the LIPAc IPM, however, the ionization current is directly measured on strip cathodes to improve the radiation hardness of the IPM.

Due to their principle of operation, IPMs are intrinsically prone to profile distortion caused by deformations of the ionization particle density during the drift towards the read-out plate. The most obvious source of such deformations is the extraction field itself. The design of the field box is therefore of utmost importance for the IPM as it guarantees the uniformity of the extraction field. To counteract other effects, like initial particle velocities or the beam's space charge, a magnetic field parallel to the electric extraction field can be used to confine the ionization particles. As the magnetic field strongly affects the beam as well and since therefore compensation magnets have to be set up, such a solution is spacious and not feasible due to the tight space limitation of LIPAc [5]. The LIPAc IPM will therefore collect ions on cathode strips with an electric extraction field only.

LIPAC IPM PROTOTYPE DESIGN

To investigate features and properties of IPMs, a prototype has been designed, built, and tested [6, 7]. A photo of this prototype after the tests is given in Fig. 1. On top, there are 32 strip cathodes with a spacing of 1.25 mm to read the ionization current. To vary the active depth of the IPM, the strips can be shielded by metal plates that only leave a slit of variable size open, through which ions can reach the strip cathodes. On the bottom plate, a positive high voltage is applied by which the ions are accelerated towards the strips. On both hand sides of the IPM, there is a total of 6 degraders which are set on appropriate voltages to reduce fringe fields. Additional electrodes in the form of wires on top and on bottom outside the IPM field box reduce fringe fields in beam direction. *Finite Element Method (FEM)* simulations indicate an electric field uniformity within 3 % [8].

Three different front-end electronics are available, one linear and one logarithmic card

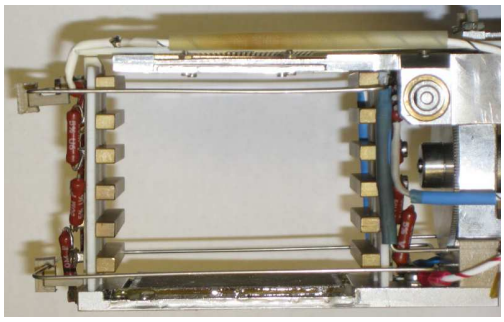

FIG. 1. Photo of the LIPAc IPM prototype.

based transimpedance amplifiers, and another card based on charge integration. Each of these cards provides a multiplexed output; for the two cards based on amplifiers, profiles are taken every 2 μs. All front-end electronic cards were designed at CEA Saclay.

PROTOTYPE TESTS

The IPM prototype was extensively tested during two campaigns at the *UNILAC (UNIversal Linear ACcelerator)* at GSI and at the *SILHI (Source d'Ions Légers à Haute Intensité)* at CEA Saclay. At the UNILAC, the prototype was tested at pulsed heavy-ion beams of low and intermediate intensity (30 μA - 1.6 mA) and at the SILHI, it was tested at proton beams of high intensity (2 mA - 20 mA) in cw and in pulsed mode at high duty cycle .

Tests at UNILAC

The IPM prototype was tested at the X2-branch of the UNILAC at GSI in two campaigns in May 2010 and November 2010. The X2-branch is dedicated to the test of diagnostics and is equipped with various diagnostics devices including a gas inlet system of the *Beam Induced Fluorescence (BIF)* monitor that proved to be particularly useful for our tests as well. The gas inlet system did allow to vary not only the residual gas pressure, but also the residual gas atom type.

Extraction Field Uniformity

It was one of the main objectives of the prototype design to achieve a good uniformity of the electric extraction field. To test the electric field uniformity, the IPM prototype was mounted on a stepper motor and moved perpendicular to a 33 μA Ca^{10+} beam. The profile shift versus the IPM displacement is given in Fig. 2. One can see that the prototype is highly linear over its entire active area.

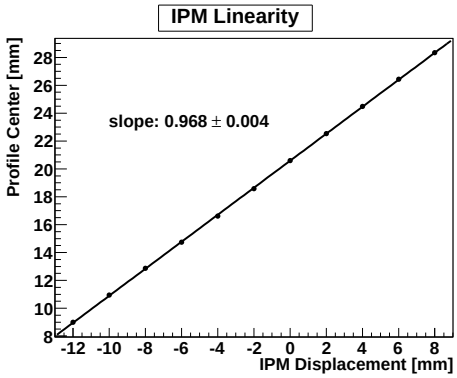

FIG. 2. Profile shift versus IPM displacement over the entire active range.

Spacial Resolution

The very same technique can be applied to determine the resolution of the profile center by reducing the step size with which the IPM was moved. As shown in Fig. 3, our prototype can well resolve beam shifts of 100 μm. Profiles for this analysis have been acquired from a 1 mA Xe^{21+} beam.

The resolution of the profile center highly depends, of course, on the statistics of the data available, which in turn depends on integration time, beam current, and residual gas pressure. In Fig. 4, the RMS fluctuation of the profile center is plotted versus the time of data taking for a 120 μA Xe^{21+} beam at a residual gas pressure of 10^{-5} mbar. The RMS value drops with longer integration times until it reaches a plateau of about 100 μm at read-out rates of the order of 1 kHz. There are bumps in the curve every 200 μs which corresponds to the beam pulse length. This indicates that the determined resolution limit of 100 μm might possibly still be determined by beam fluctuations.

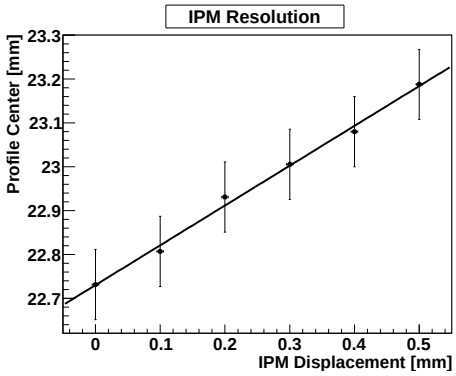

FIG. 3. Profile shift versus IPM displacement in 100 μm steps.

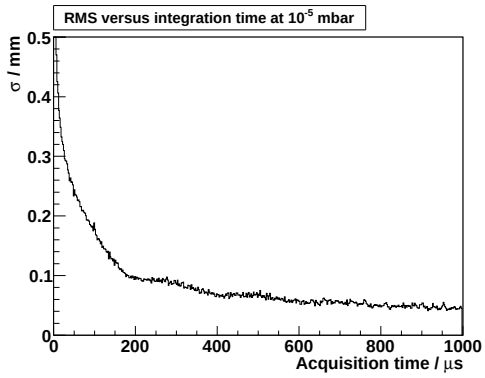

FIG. 4. RMS fluctuation of the beam profile center versus time of data taking.

Profile Distortion Effects

The high linearity of the IPM and the good resolution of the profile center confirm the uniformity of the electric extraction field. It still remains to investigate effects that do not affect the profile center, but distort the profile shape nonetheless, like initial ion velocities after the ionization process or the beam's space charge. By varying the extraction field strength, one can vary the effect that such processes have on the measured profile. The profile width of a 1 mA Xe^{21+} beam plotted versus the extraction field strength for various residual gases is given in Fig. 5. For noble gases as residual gas, the profile width reaches a constant value at few 100 V/cm. At this point, the extraction field dominates any distortion process and since it is considered uniform, the measured profile corresponds to the actual beam profile.

However, for the molecular nitrogen, plotted in different scale, the profile width hardly reaches a constant value. As the effect of the space charge is expected to be identical for

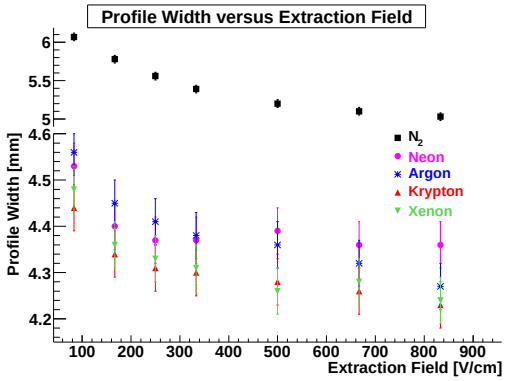

FIG. 5. Profile of a 1 mA Xe^{21+} beam versus extraction field strength for various residual gases.

nitrogen and on noble gases, it could be concluded that the dominating broadening effect is not the space charge but the initial particle velocities. Assuming that molecules receive a higher momentum transfer during the ionization process, one could explain the stronger profile broadening.

Signal Amplification

During these measurements, it was seen that the IPM signal increased with stronger extraction fields. The profiles have been integrated and the resulting total IPM signal was plotted versus the extraction field. A linear fit was performed which is given in Fig. 6. Slope and y-intercept of the linear fits strongly differ for the different residual gases.

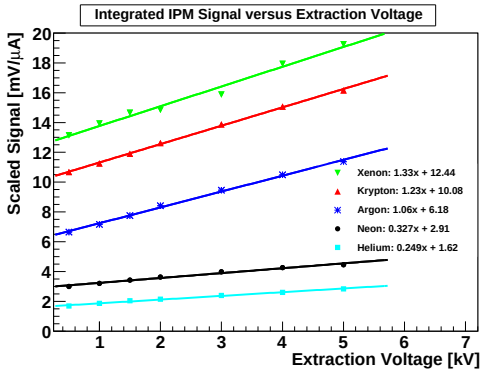

FIG. 6. Integrated profiler signal versus extraction field strength.

We propose *Secondary Electron Emission (SEM)* on the read-out strips as explanation for this signal amplification effect and have calculated the SEM yields, the average number

TABLE I. Normalized SEM yields required to explain the signal amplification effect of the IPM compared to literature values. All SEM yields are scaled on the mean value of the yields for Ne, Ar, and Kr.

	Magnuson [9]	Carston [10]	Zalm [11]	Baragiola [12, 13]	IPM
He	—	—	—	1.47	1.47
Ne	1.14	0.97	1.13	—	1.06
Ar	0.95	1.06	0.94	1.06	1.15
Kr	0.91	0.97	0.94	0.94	0.79
Xe	0.64	0.64	0.61	—	0.61

of electrons emitted per incident ion, required for the observed amplification effect. SEM yields for heavy ion bombardment are available in literature for various target materials, projectile types and energies [9–13]. However, such SEM yields are determined for carefully cleaned and rinsed material samples, and already thin oxidation layers are reported to have a tremendous impact on the secondary electron emission [14]. To compare our calculated SEM yields with literature values nonetheless, we assume the effect of any oxidation layer to be linear and scale the determined SEM yields on a mean value. As literature values of SEM yields for Ne, Ar, and Kr are mostly available, it was decided to use their mean as appropriate scaling. The SEM yields from Baragiola et al. are scaled on Ar and Kr only as no value for Ne was found. The scaled SEM yields required to explain the signal amplification effect of the IPM compared to scaled literature values are presented in Table I.

The SEM yields required to explain the signal amplification of the IPM prototype scaled on a mean value match literature values well within 20 %. The error expected from our measurement setup that was not designed for such kind of test can be expected to be well above these 20 %. It can be concluded that a signal amplification due to secondary electron emission on the read-out strips is campatible with our measurement.

Profile Comparison

It was shown that the electric extraction field is uniform, that it dominates any other distortion mechanism at nominal field strength and that the measured profile therefore

should be the real beam profile. To test this in a more direct manner, we have compared profiles of 1 mA Xe^{21+} beams acquired by our IPM with profiles from a BIF monitor of GSI [15]. In Fig. 7, an IPM profile is given in blue and a BIF profile in red. The profiles match nicely as indicated by the calculated standard deviations of 4.72 mm for the IPM and 4.73 mm for the BIF profile. Additional IPM and BIF profiles have been compared for various residual gas types and pressures. The RMS width of IPM and BIF profiles commonly match well within 100 μm.

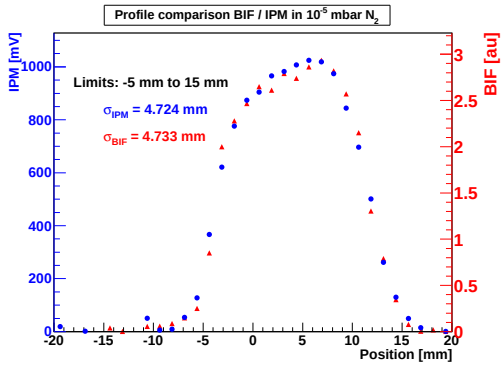

FIG. 7. IPM profile (blue) and BIF profile (red) are in good agreement.

Tests at SILHI

At the UNILAC at GSI, we have tested our IPM prototype at pulsed heavy-ion beams of low and intermediate intensity. As the final IPM must handle the 125 mA cw beam of the LIPAc, the tests at GSI do not suffice, but the IPM prototype had to be tested at cw beams of intensity as well.

At SILHI at CEA Saclay, we have operated the IPM prototype at 90 keV cw proton beams of up to 10 mA. In terms of charge density, this corresponds to 70 mA deuteron beams of 9 MeV, the LIPAc energy. At higher beam currents, the power supply of the IPM field box started tripping. We assume that we have extracted electrons from the beam and collected them on the high-voltage plate of the IPM. As electrons are used in high-current injectors to reduce the beam space charge, this effect is not to be expected for the final IPM.

FINAL IPM DESIGN

Based on the findings of the tests at the UNILAC and the SILHI, the final versions of the LIPAc IPMs have been developed, with an apertures of 103 mm and 153 mm. For the IPMs, only radiation hard materials have been used, like metals, ceramics, epoxy glass, etc. A sketch of the final IPM with 153 mm aperture is given in Fig. 8.

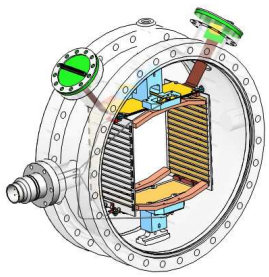

FIG. 8. Design of the final LIPAc IPM.

The internal aperture of the IPM is a few mm larger than the internal beam pipe diameter. This way, the IPM is well protected by the beam pipe itself. This approach however places the circular beam pipe in close proximity to the rectangular field box. To counteract any distortions of the electric extraction field caused by the grounded beam pipe, the wire electrodes of the IPM prototype have been replaced by curved electrodes on both sides of the IPM, as can be see seen in Fig. 8 in a copper-like color.

The IPM field box was designed to optimize the electric field uniformity based on FEM simulations by Lorentz-E [8] while keeping the IPM depth within reasonable limits. This process includes the adjustment of size, position and voltage of each degrader pair and optimization of the curvature, size and voltage of the correction electrodes. The electric field was found to be uniform within 1.5 % in most of the active area.

For a better understanding of the extraction of the ionization particles by the electric field, a particle tracking was performed. The transverse displacement of the extracted ions in the central IPM plane in plotted in Fig. 9. Since no particles are expected outside the beam pipe diameter, the drift is set to zero in this region. One can see that in the center of the beam pipe, where the beam is to be expected, the transverse ion drift is constantly well below 500 μm.

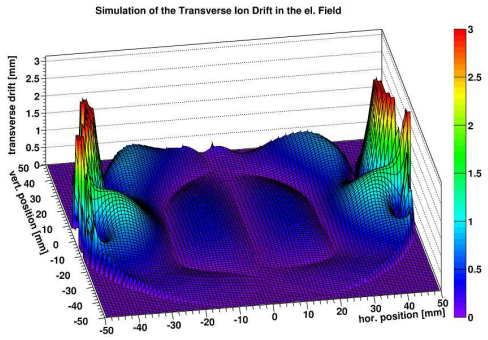

FIG. 9. Transverse ion displacement during their drift towards the read-outstrips in the extraction field only.

SPACE CHARGE EFFECT

This particle tracking, however, only takes into account the effect of the electric extraction field, but not the space charge field. Using a "point summation" technique the space charge field of a 125 mA cw beam has been calculated for a beam distribution provided by our beam dynamics group. The resulting space charge field was superimposed with the field of the IPM field box, and the particle tracking was repeated. The resulting ion displacement in a different scale is given in Fig. 10.

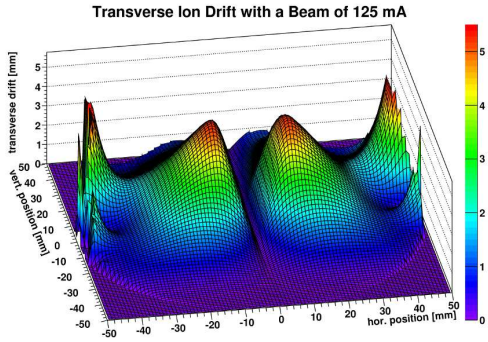

FIG. 10. Transverse ion displacement during their drift towards the read-outstrips in the extraction and the space charge field.

The extraction field does not longer dominate the extraction process, but the space charge field results in an ion displacements of over 5 mm. The IPM will therefore measure a profile which is much broader than the actual beam profile. A simulation of such a measurement is given in Fig. 11.

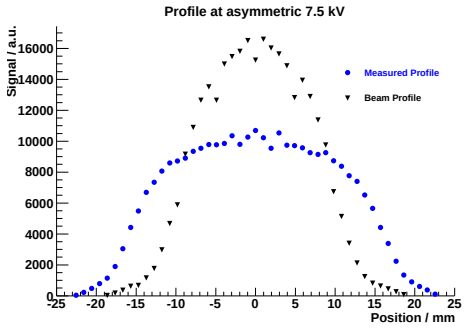

FIG. 11. Simulation of a measured profile of a 125 mA beam (blue) in comparison to the actual beam profile (black).

SPACE CHARGE COMPENSATION

Since no magnetic field can be applied due to a lack of space to confine electrons, other techniques have to be developed to overcome the space charge effect. Increasing the electric field will reduce the effect of the space charge, but this was found to be not sufficient for a proper profile measurement. Another approach that shows more merit is a correction algorithm that folds back the broadened profile to correct for the space charge effect.

Such a space charge compensation algorithm requires the beam distribution as input to calculate the space charge field. The algorithm is implemented such that it assumes a random beam particle distribution to perform a particle tracking for this distribution and to determine the probability for each ion collected on the strips where it might have been created. Based on these probabilities, a correction matrix is calculated that can be multiplied on the vector of the measured profile to derive the actual beam profile.

If the resulting corrected profile differs from the profile of the beam particle distribution used as input, the calculation is not self-consistent and a new beam particle distribution is tested. This can be repeated until a self-consistent solution is found. By generating a database of correction matrices for possible beam particle distributions, such a compensation algorithm could be applied even on-line.

This technique has only been tested in simulation so far and still is in a very preliminary state. To reduce any distortions due to malfunctioning of the algorithm, we consider to increase the extraction field strength. The practical feasibility of such an algorithm will be tested at the SILHI in November 2011. For this test it is foreseen to vary the extraction

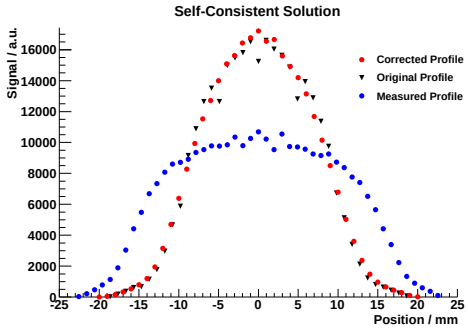

FIG. 12. A space charge compensation algorithm applied on a simulated profile measurement (blue) can grant a corrected profile (red) which is in good agreement with the original beam profile (black).

voltage and to reconstruct the profile independently for various extraction voltages. A malfunctioning algorithm would result in deviations of the reconstructed profiles and deviations of the reconstructed profiles can serve as indication for the reliability of this technique. This could also be done at LIPAc to validate acquired profiles and to thereby limit the effect of an algorithm failure.

CONCLUSION AND OUTLOOK

We have designed, built, and tested a prototype for the LIPAc ionization profile monitor. It was tested at the UNILAC at GSI and at the SILHI at CEA Saclay. The performance of the prototype exceeded our expectations and its properties are well understood by now. Based on our findings, we have designed the final LIPAc IPMs, out of which one is already manufactured and will be tested at SILHI in November 2011. During this test, the feasibility of a space charge compensation algorithm will also be tested that is supposed to compensate for the space charge effect.

ACKNOWLEDGMENTS

We would like to express our sincere thank to the diagnostics staff of GSI and to the SILHI group for continuous support and advice during the measurements.

The work is supported by DITANET, a Marie Curie Action of the E.U., contract PITN-

GA-2008-215080.

[1] P. Forck, A. Bank, T. Giacomini, and A. Peters, in *Proc. of DIPAC05* (2005).

[2] P. Garin and M. Sugimoto, Fusion Engeneering design **84**, 259 (2009).

[3] I. D. Kaganovich, E. Startsev, and R. C. Davidson, New Journal of Physics **8**, 278 (2006).

[4] W. H. DeLuca, IEEE Trans. Nucl. Sci. **16-3**, 813 (1969).

[5] T. Giacomini, P. F. D. Liakin, J. Dietrich, and G. v. Villiers, in *Proc. of DIPAC2011* (2011).

[6] J. Marroncle, P. Abbon, F. Jeanneau, J.-P. Mols, and J. Pancin, in *Proc. of DIPAC09* (2009).

[7] J. Egberts, P. Abbon, F. Jeanneau, J. Marroncle, J.-P. Mols, T. Papaevangelou, F. Becker, P. Forck, and B. Walasek-Höhne, in *Proc. of DIPAC2011* (2011).

[8] "Lorentz-E Three-Dimensional Particle Trajectory Solver (Electric)," Copyright 1998 - 2010 Enginia research Inc.

[9] G. Magnuson and C. Carlson, Physical review **129**, 2403 (1963).

[10] C. E. Carlston, G. Magnuson, and P. Mahadevan, Physical Review **139**, A729 (1965).

[11] P. Zalm and L. Beckers, Journal of Surface Science **152**, 135 (1985).

[12] R. A. Baragiola, E. V. Alonso, and A. Oliva-Florio, Physical Review B **19**, 121 (1979).

[13] R. A. Baragiola, E. V. Alonso, J. Ferron, and A. Oliva-Florio, Journal of Surface Science **90**, 240 (1979).

[14] J. Ferron, E. V. Alonso, R. A. Baragiola, and A. Oliva-Florio, Journal of Surface Science **120**, 427 (1982).

[15] F. Becker, A. Hug, P. Forck, M. Kulish, S. Udera, and D. Varentsov, Laser and Particle Beams **24**, 1 (2006).